PNAS RESEARCH ARTICLE | CHEMISTRY

Colorful low-emissivity paints for space heating and cooling energy savings

Yucan Peng[a,1], Jian-Cheng Lai[b,1], Xin Xiao[a], Weiliang Jin[c], Jiawei Zhou[a], Yufei Yang[a], Xin Gao[a], Jing Tang[a], Lingling Fan[c], Shanhui Fan[c], Zhenan Bao[b], and Yi Cui[a,d,2]

Edited by Peidong Yang, University of California Berkeley, Berkeley, CA; received January 23, 2023; accepted July 2, 2023

Space heating and cooling consume ~13% of global energy every year. The development of advanced materials that promote energy savings in heating and cooling is gaining increasing attention. To thermally isolate the space of concern and minimize the heat exchange with the outside environment has been recognized as one effective solution. To this end, here, we develop a universal category of colorful low-emissivity paints to form bilayer coatings consisting of an infrared (IR)-reflective bottom layer and an IR-transparent top layer in colors. The colorful visual appearance ensures the aesthetical effect comparable to conventional paints. High mid-infrared reflectance (up to ~80%) is achieved, which is more than 10 times as conventional paints in the same colors, efficiently reducing both heat gain and loss from/to the outside environment. The high near-IR reflectance also benefits reducing solar heat gain in hot days. The advantageous features of these paints strike a balance between energy savings and penalties for heating and cooling throughout the year, providing a comprehensive year-round energy-saving solution adaptable to a wide variety of climatic zones. Taking a typical midrise apartment building as an example, the application of our colorful low-emissivity paints can realize positive heating, ventilation, and air conditioning energy saving, up to 27.24 MJ/m^2/y (corresponding to the 7.4% saving ratio). Moreover, the versatility of the paint, along with its applicability to diverse surfaces of various shapes and materials, makes the paints extensively useful in a range of scenarios, including building envelopes, transportation, and storage.

low-emissivity paint | colorful | radiative heat insulation | energy saving | carbon neutrality

Maintaining thermal environments with temperature in a certain range is substantial for human society, which not only directly influences human body thermal comfort and work efficiency (1, 2) but also plays an important role in storage and transportation (3). A huge amount of energy is consumed every year for evacuating or resisting extra heat gain and loss to/from spaces of concern to preserve suitable thermal environments (4, 5), generating an enormous amount of greenhouse gases (6, 7). For example, buildings contribute to about 40% of total energy consumption in the United States (8–10), and their heating, ventilation, and air conditioning (HVAC) systems account for around 40% of building energy end use (11); The cooling expenses for cargo transportation can take up of 50% of the total transportation charges (12). Accordingly, how to effectively reduce heat exchange between the concerned space and its ambient is gaining increasing attention, and novel materials for enhanced thermal insulation are in demand.

Different from radiative cooling strategy taking advantage of the cold universe for maximized heat dissipation, improved heat insulation can generally benefit both cooling and heating energy saving, which is applicable to locations in various climate zones and during different seasons. Materials of low thermal conductivity suppress heat conduction by trapping air in their highly porous structure, such as fiberglass, cellulose, polymeric foam, and aerogels (13, 14), and by further reducing the gas molecule collision through air evacuation, such as vacuum insulation panels (15). They are often installed with centimeters of thickness within the envelopes of enclosed spaces to provide extra heat insulation (16). In contrast, radiant barrier insulation materials are endowed with engineered optical properties, which show desired control for received radiation at the surface (17, 18). For instance, aiming at transparent envelopes, significant efforts have been made to develop low-emissivity (low-e) glass and flexible low-e window films for retrofit (19), which are designed to cut down infrared (IR) radiation but remain visibly transparent. For opaque envelopes, demonstrated strategies include installing metalized/metal foils within walls (20), using hollow bricks with reflective inner surfaces (21), and applying paints containing heat-reflective metal materials (22, 23).

However, the state-of-the-art low-e materials typically used for opaque envelopes are often designed to have high reflectance in both visible and IR wavelengths. This usually gives them

Significance

Aiming at providing a conventional paint alternative and a universal energy-saving solution, we have developed colorful low-emissivity paints. They can be used to create bilayer coatings that exhibit low emissivity (i.e., high reflectance) in infrared (IR) wavelengths while showing colorful visual appearance. High mid-infrared reflectance significantly enhances radiative heat insulation for enclosed spaces, effectively resisting heat gain or loss from/to the external environment. Meanwhile, high near-IR reflectance mitigates solar heat gain during hot weather. Beyond aesthetical appeal, the optical design establishes an effective balance between energy savings and trade-offs associated with heating and cooling, reducing annual energy consumption for maintaining indoor thermal environments. As a result, our strategy offers advantages for space heating/cooling energy saving and carbon neutrality.

Author contributions: Y.P. and Y.C. designed research; Y.P., J.-C.L., X.X., W.J., Y.Y., X.G., J.T., and L.F. performed research; Y.P., X.X., W.J., J.Z., S.F., Z.B., and Y.C. analyzed data; S.F., Z.B., and Y.C. supervised the project; and Y.P., J.-C.L., S.F., Z.B., and Y.C. wrote the paper.

Competing interest statement: This work has been filed as a US patent (Appl. No.: 63/355193).

This article is a PNAS Direct Submission.

[1]Y.P. and J.-C.L. contributed equally to this work.

[2]To whom correspondence may be addressed. Email: yicui@stanford.edu.

This article contains supporting information online at https://www.pnas.org/lookup/suppl/doi:10.1073/pnas.2300856120/-/DCSupplemental.

Published August 14, 2023.

a metallic silver or gray color, resulting in significant aesthetic limitations. (24). They are restricted to be used where decorative appearance is not a concern, such as loft spaces or cavity wall voids as mentioned above (23). In practical application, the aesthetical effect provided by colors is considered important as or even more critical than the thermal effect provided by materials. Colors shape the appearance of environments, satisfy people's visual experience, and afford necessary symbolism in certain circumstances (25, 26). The importance of colors attracts attention when new materials are developed (27–30). For instance, aiming at enhancing thermal insulation, we recently developed low-e thin films with a range of visual colors for building wall application (30). Nevertheless, the thin film form still imposes limitations on the scope of its applications. The development of colored low-e materials that can be more broadly applied in practical energy-saving applications continues to be a significant challenge.

Here, aiming at providing a universal energy-saving solution, we propose a category of colorful low-emissivity paints serving as conventional paints alternative. They show high installation flexibility for surfaces of various shapes and materials. Furthermore, they are versatile, suitable for a variety of application scenarios including buildings, transportation, storage, and packaging. The paints not only satisfy the basic functions of conventional paints but also decrease thermal radiation exchange to save either heating or cooling energy. Taking building envelope as an example, as illustrated in Fig. 1*A*, these paints are designed to create coatings on envelope surfaces such as walls and roofs to help prevent thermal radiation exchange with surroundings located in the mid-infrared (MIR) wavelength range (mainly 7 to 14 μm). In hot weather, the coating decreases the thermal radiation throughput from the hot ambient and from the solar near-infrared (NIR) radiation to reduce heat gain; In cold weather, the coating impedes MIR radiative heat loss from the indoor environment to the outdoor surroundings. Meanwhile, colorful appearance is realized as well by selectively reflecting visible light of the desired color. In other words, the formed coating is targeted at enhancing radiation heat transfer resistance to benefit space cooling and heating energy efficiency without sacrificing the comparable visual appearance to conventional paints.

Results and Discussion

Material Design. To achieve this goal, we conceive a bilayer coating structure with desired optical property, which can be facilely prepared by the spray coating method (Fig. 1*B*). We design an IR-reflective layer as the bottom layer to produce high IR reflectance, thus resisting

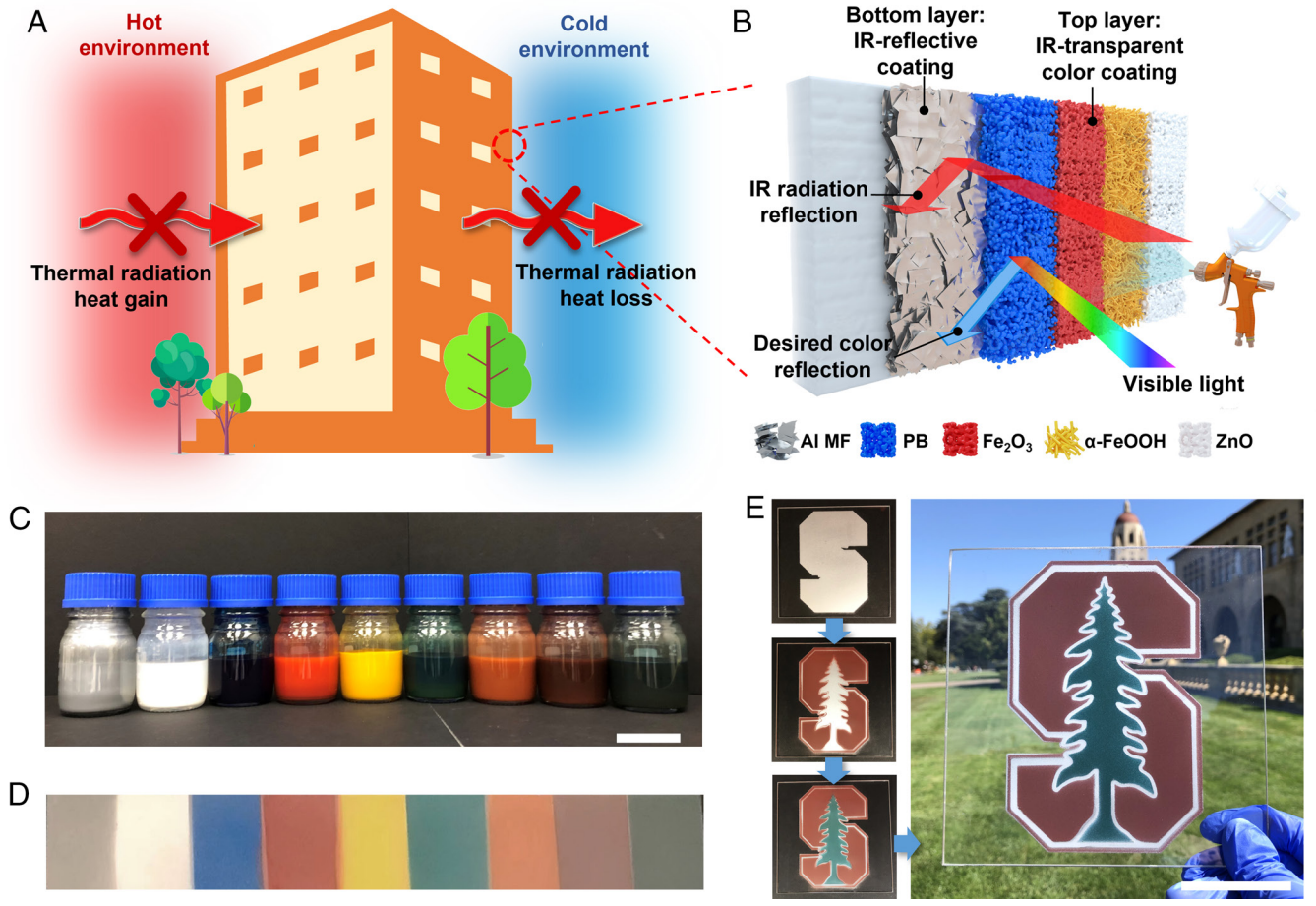

Fig. 1. Schematic illustration of design principle and exhibition of samples. (*A*) Graphical explanation of the working mechanism of the colorful low-emissivity paints. The paints resist thermal radiation exchange with hot environment to reduce heat gain and with cold environment to decrease heat loss. This category of paints is not only suitable for thermal envelopes of buildings as depicted but applicable to other objects as well. (*B*) Schematic explanation of the designed bilayer structure for applying the paints. The bottom layer is IR reflective coating, which is based on Al MFs. The top layer is IR-transparent color coating, which creates desired visual appearance but hardly destroys the high IR reflectance resulted from the bottom layer. PB, Fe_2O_3, α-FeOOH, and ZnO are utilized for blue, red, yellow, and white colors, respectively. (*C*) Photograph of the formulated paint solutions for bottom layer (far left one) and for top layer (in various colors: white, blue, red, yellow, green, orange, purple, and dark gray, from left to right, respectively). (Scale bar, 5 cm.) (*D*) Photographs of the bottom layer coating (far left one) and bilayer low-e coatings (BLCs) in various colors produced by the paint solutions. (*E*) Photographs showing the fabrication process of and the final produced Stanford logo using our colorful low-emissivity paints. (Scale bar, 5 cm.)

heat gain and loss by significantly reducing MIR thermal radiation absorption and emission. Also, it decreases NIR heat gain from the sun. The top layer serves as an IR-transparent color layer, selectively reflecting desired visible colors but allowing high transmission of IR radiation to retain the high IR reflectance of the bottom layer. Accordingly, two groups of paints that can be readily used to form the proposed bilayer coatings are developed. The IR reflective aluminum (Al) microflake (MF) paint that can create the heat-reflective coating is formulated (far left one, Fig. 1 *C* and *D*). The IR-transparent colorful paints based on inorganic nanoparticles are formulated in assorted colors for the colorful top layer coating (others, Fig. 1 *C* and *D*). Prussian blue (PB), iron oxide (Fe_2O_3), goethite (α-FeOOH), and zinc oxide (ZnO) are utilized to generate primary colors (blue, red, yellow, and white, respectively), by which other colors can be created through mixing. The colorful low-e paints, incorporating the above two groups of paints, are appropriate replacements for conventional paints. They not only maintain the aesthetic effect, but also provide additional heat insulation. Desired graphic patterns in various colors can be easily created. Fig. 1*E* exhibits photographs of the fabrication process and the prepared Stanford logo with bilayer structure achieved using our paint solutions, which demonstrates that they can be promising alternatives for conventional paints. In Movies S1 and S2, we show the spray coating and drawing processes to create different patterns, further exhibiting the application flexibility of our colorful low-emissivity paints.

More specifically, low-cost micro-sized Al flakes (dozens of μm in the lateral dimension) are employed as the functional component of the heat-reflective paint for the bottom layer. They are dispersed in a binary solvent system (p-Xylene and methylene chloride) with dissolved Nitrile Butadiene Rubber-co-Urea (NBR-U) as the polymer binder. The Al MFs with large aspect ratio and surfactant-modified surface (31) (*SI Appendix*, Fig. S1) tend to congregate and orientate to assemble a dense and smooth surface, as shown in the scanning electron microscope (SEM) image of the Al MF coating surface morphology (Fig. 2*A*). Such an Al MF coating shows MIR reflectance of ~85% (Fig. 2*D*), which is a comprehensive outcome of selection of Al particle type, solvent and polymer binder, and their ratio optimization (see *SI Appendix*, Note S1 and Figs. S2–S4 for more details). Glass that is highly IR emissive and visible transparent was adopted as the substrate.

To retain the IR reflectance of Al MF coating meanwhile applying colors, we select inorganic IR-transparent nanoparticles as pigments to formulate the colorful IR-transparent paints (28, 32). Attenuated total reflection–Fourier transform infrared (ATR-FTIR) spectra of the selected pigments verify that these inorganic solids have negligible absorbance in the MIR wavelength range, except for an intense and narrow peak of PB at 4.8 μm due to -C ≡ N stretching vibration and two weak and broad peaks of α-FeOOH due to -OH bending vibration (*SI Appendix*, Fig. S5). Their particle sizes are in the range of 20 to 1,000 nm, which is far smaller than the MIR radiation wavelengths; thus, strong scattering can be greatly avoided for high IR transparency. One or multiple types of inorganic IR-transparent nanoparticle pigments are dispersed in the NBR-U (binder)–acetone (solvent) system. By spray coating, the nanoparticles are dispersed on the top surface of oriented Al MFs (Fig. 2*B* and *SI Appendix*, Fig. S6). The SEM image of the cross-section of a typical bilayer colored (red) low-e coating is displayed in Fig. 2*C*. A combination of Al MF layer, approximately 5 to 10 μm thick, and a color layer that is just a few micrometers thick, is sufficient to produce apparent colors and fairly high MIR reflectance. We denote the BLCs in different colors as "color"-BLC, such as blue-BLC.

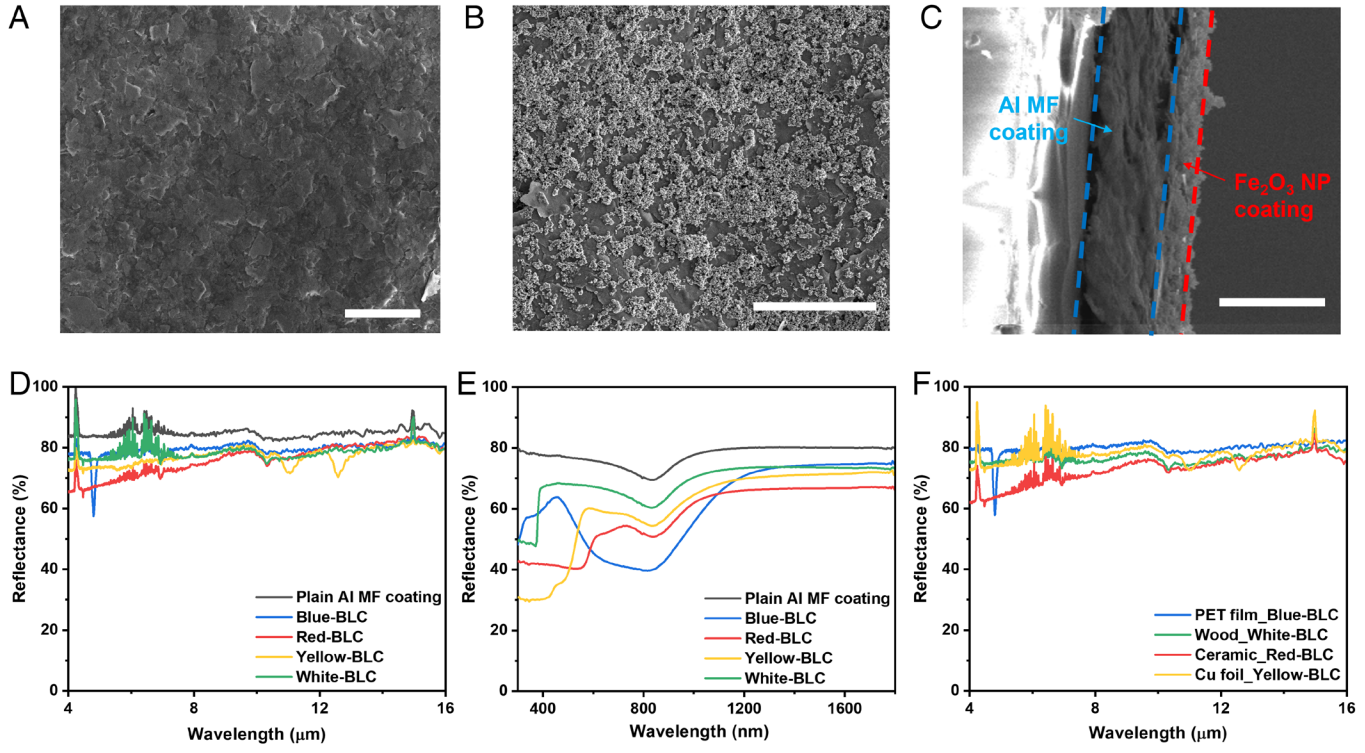

Fig. 2. Morphology and optical property characterization. (*A*) SEM image showing the surface morphology of the plain Al MF coating. (Scale bar, 50 μm.) (*B*) SEM image of the colorful (red) BLC, of which bottom is Al MF coating and top is Fe_2O_3 nanoparticle (NP) coating. (Scale bar, 20 μm.) (*C*) SEM image of the cross-section of the bilayer red low-emissivity coating. The blue dashed lines locate the Al MF coating, while the red dashed lines locate the layer of the Fe_2O_3 NP coating. (Scale bar, 10 μm.) (*D*) Measured total reflectance in the MIR wavelength range on the glass substrate for the single layer of the Al MF coating and BLCs in blue, red, yellow, and white. (*E*) Measured total reflectance in the visible and NIR wavelength ranges on the glass substrate for the single layer of the Al MF coating and BLCs in blue, red, yellow, and white. (*F*) Measured total reflectance in the MIR wavelength range for the colorful bilayer low-emissivity coatings on different substrates.

Optical Characterization. Fig. 2*D* exhibits the measured total MIR reflectance with an FTIR spectrometer equipped with a diffuse gold integrating sphere. The plain bottom layer of the Al MF coating on a glass substrate shows about 85% reflectance, equivalent to ~0.15 emissivity. The addition of the top color layer reduces the total MIR reflectance due to the inevitable thermal absorption by the polymer binder and porous morphology, but the total MIR reflectance can still reach up to ~80%. In contrast, conventional paints in the same colors show reflectance lower than 10% in the MIR wavelength range (*SI Appendix*, Fig. S7*A*), which strongly absorb thermal radiation. Besides, we measured the total reflectance of these colored low-emissivity coatings in the visible and NIR wavelength ranges with a UV-Vis-NIR spectrometer equipped with a diffuse reflectance accessory. As shown in Fig. 2*E*, the single layer of the plain Al MF coating exhibits ~80% reflectance across the whole visible and NIR wavelength ranges; The spectra of bilayer coatings in primary colors show 65 to 75% reflectance in the NIR wavelength range while revealing different dominant reflection visible wavelengths for blue, red, and yellow colors. Conventional paints also show selective reflectance peaks corresponding to their colors, whereas their reflectance in both visible and NIR wavelengths is overall much lower (*SI Appendix*, Fig. S7*B*). It is worthwhile to point out that changing the loading mass of the colorful coating can result in varied shades for different colors. Even though some spectra variation is observed, fairly high IR reflectance can be retained even for very dark shades (*SI Appendix*, Fig. S8). The measured spectra of bilayer coatings in colors generated by mixing pigments for primary colors are displayed in *SI Appendix*, Fig. S9.

Besides, we examined the thermal radiation reflection performance of the formulated colorful low-e paints on different substrates (plastics, wood, ceramics, metal, and glass). *SI Appendix*, Fig. S10 shows the measured MIR reflectance of the plain Al MF coating on different materials, in addition to the glass substrate used above. It is observed that almost identical MIR reflectance is achieved on all the tested materials. This is because the Al MF paint for bottom-layer coating can well match different substrates and alter their surface morphology to be similar to congregated and oriented Al MF assembly. As a result, the MIR reflectance for colorful BLCs on varied substrates exhibits similar spectra to those on the glass substrate, as displayed in Fig. 2*F*.

Evaluation of Practical Application Feasibility. Furthermore, the feasibility of practical usage is verified through characterization of surface properties as well as optical properties. First, water contact angles are measured for both the plain Al MF coating and bilayer coatings. As exhibited in Fig. 3*A*, the coatings show an average water contact angle of 118°. This decent hydrophobicity indicates the coatings repel water, which potentially enhances its stability in humid environments. To evaluate the durability of coatings in different environments, the coating samples were preserved in high temperature (80 °C), low temperature (liquid nitrogen), acid (sulfuric acid, pH = 4), and alkali (potassium hydroxide, pH = 10) continuously for one week. We measured MIR spectra and observed visual appearance of samples before and after every test. The MIR spectra were unaffected after high temperature and low temperature tests (Fig. 3*B*), and the photographs demonstrate that the appearance of the coating stayed intact (*Inset* of Fig. 3*B*). The MIR spectra and appearance of coating samples were sustained well after exposure to acid and alkali as well (Fig. 3*C*). These results illustrate the fair environmental durability of the bilayer coatings. Also, the color fastness was verified by the test displayed in the inset of Fig. 3*D* in which the coating was flushed by continuous water

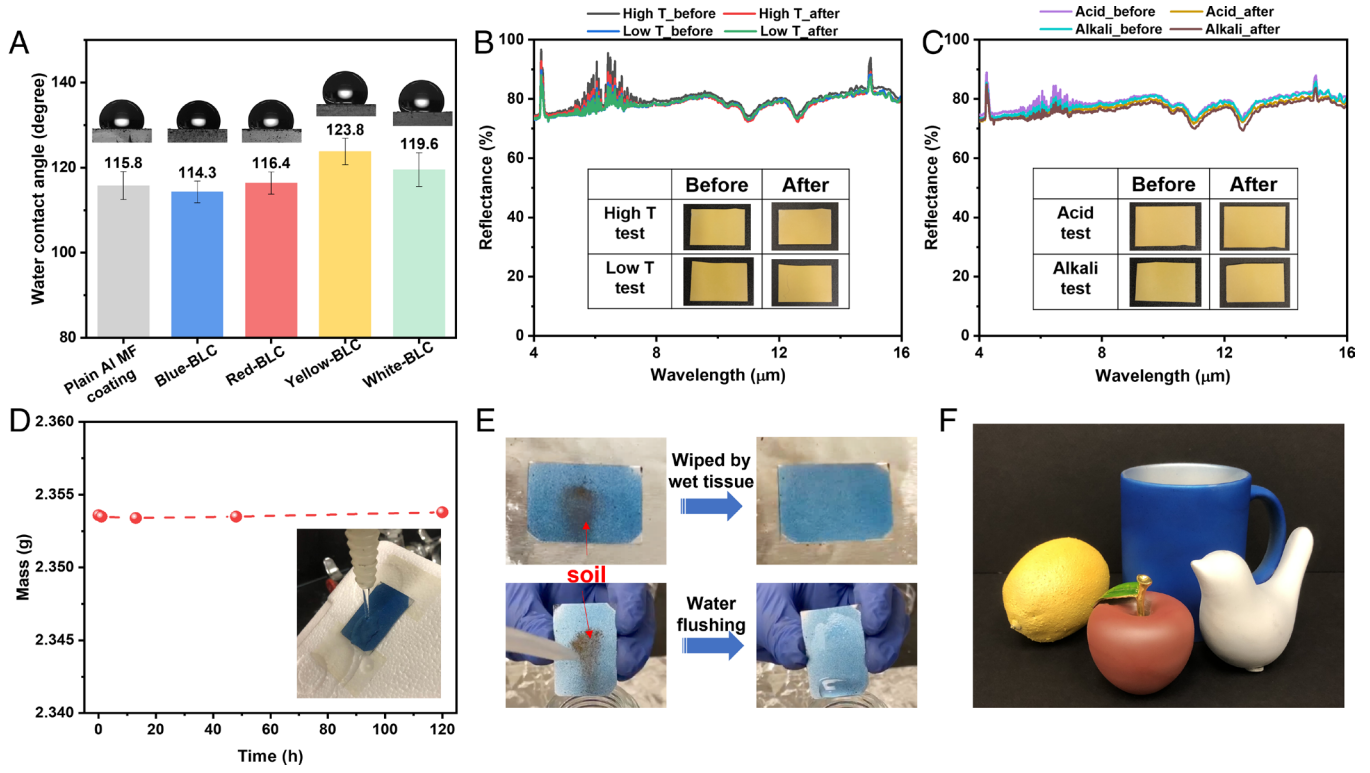

Fig. 3. Evaluation of practical application feasibility. (*A*) Measured water contact angles for the plain Al MF coating and BLCs in different colors. All the samples show decent hydrophobicity. The error bars indicate the SD values of multiple measurements. (*B* and *C*) Measured MIR spectra for samples before and after the high/low-temperature test (*B*) and acid/alkali test (*C*). No obvious spectra change was observed. The *Inset* exhibits photographs of samples before and after tests, demonstrating that visual appearance was retained as well. (*D*) Measured sample mass during the color fastness test by continuous water flushing. The sample mass was almost unchanged. (*E*) Photographs showing contaminated samples can be easily cleaned by wet issue wiping and water flushing. (*F*) Photograph of objects of different materials in various shapes, coated with our colorful low-e paints.

flow and the sample mass was measured. As shown in Fig. 3*D*, the sample mass was almost unchanged during the test, revealing that decent adhesion was achieved among the particles/flakes to prevent color fade. Moreover, the coating surface can be easily cleaned by wet tissue or water flushing (Fig. 3*E* and Movies S3 and S4). Our paint is also versatile to be applied onto assorted surfaces of various shapes and materials (Fig. 3*F*), serving as an extra thermal barrier in many different scenarios.

Heat Insulation Effect Demonstration. Then, the thermal performance in the heat insulation effect of the coatings was investigated. Building simulants were constructed, each fitted with an inserted electric heater capable of generating heat. The outer surfaces of these simulants were treated in one of four ways: unmodified, coated with a commercial blue paint coating, coated with a single layer of plain Al MF coating, or coated with the blue-BLC, respectively (Fig. 4*A*). As illustrated in Fig. 4*B*, we measured the required power density of the heater to resist heat loss and maintain the same inside temperature of the building simulants at constantly 25 °C (measured by inserted thermocouples in the building simulants) in a cold environment (5 °C). The positions of heaters and thermocouples were both identical in every building simulant for different coating samples, for parallel comparison. The plain Al MF coating and blue-BLC can both significantly reduce the heater power density in demand, compared to the blank building simulant and commercial blue paint (Fig. 4*C*). Compared to the commercial blue paint, blue-BLC decreased the required heater power density by about 36%. It validates the reduction of heat exchange with the ambient environment and great potential of building energy saving.

Owing to the installation flexibility and versatility, our colorful low-emissivity paints are suitable to be used in other scenarios that require thermal regulation. For example, they can be used on cargo trucks for cold-chain transportation, preserving inside goods with less cooling energy consumption meanwhile providing vast flexibility of truck's appearance design. Besides, the cargo trucks will be burdened with almost no extra weight and volume. As shown in Fig. 4*D*, we prepared three cargo truck models with painted cargo boxes (three faces) by the commercial white paint, Al MF paint, and white-BLC, respectively. They were tested in an artificial hot environment (40 °C).

The white-BLC was expected to afford a similar heat insulation effect to the Al MF paint, whereas it can ensure the same aesthetical effect as the commercial white paint. To demonstrate their heat resistance performance, we first measured the increase of inside

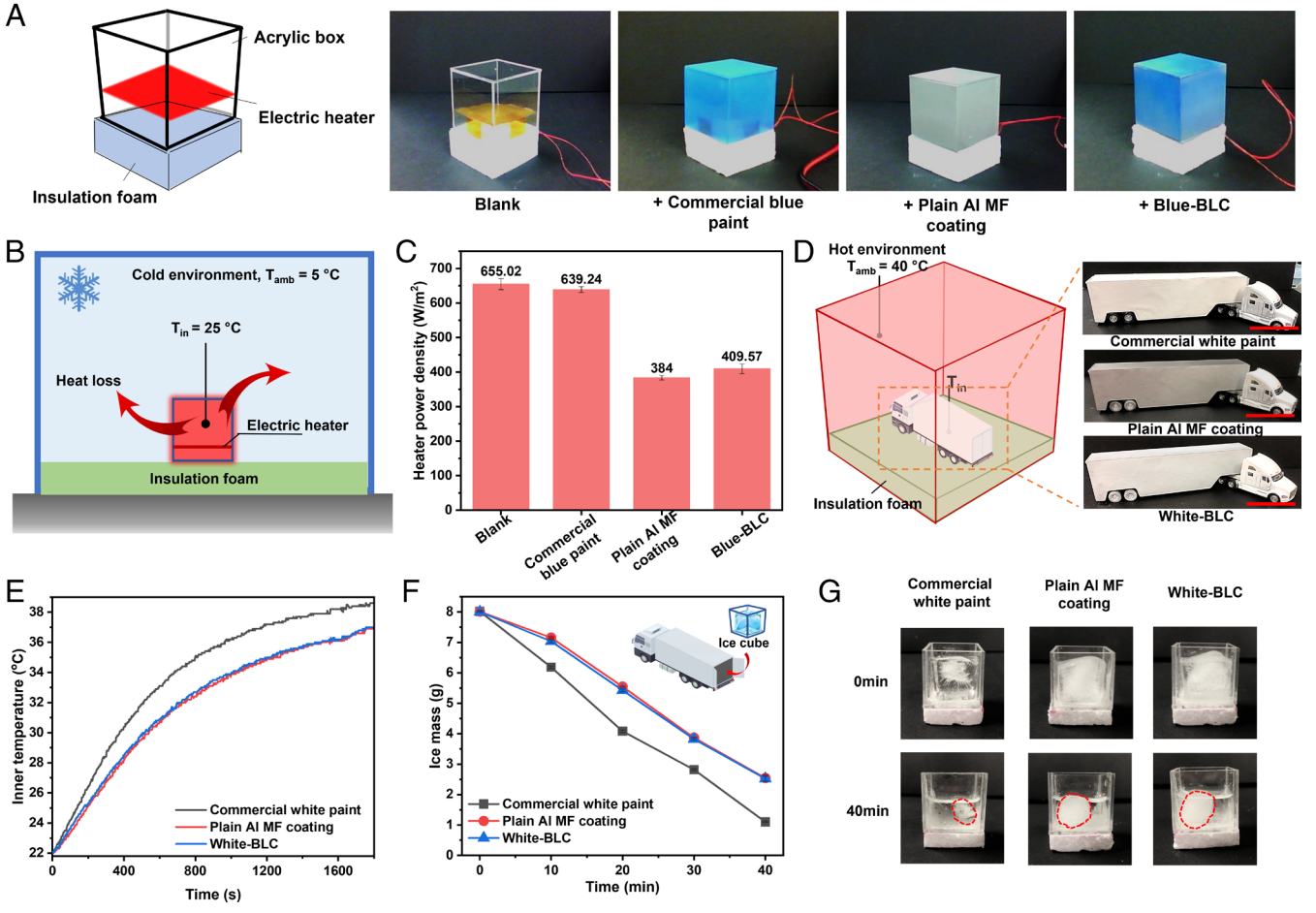

Fig. 4. Heat insulation demonstration in artificial cold/hot environments. (*A*) Schematic of the tested building simulant with inserted electric heater and the photographs of ones with different surface coatings. (*B*) Schematic illustration of the heat loss test in a cold environment. The power density of heaters was adjusted to maintain the inside temperature constantly at 25 °C. (*C*) Measured required power density of heaters. The plain Al MF coating and blue-BLC both significantly decreased the power density in need. It means that they can effectively help reduce indoor heat loss to the ambience. (*D*) Schematic illustration of the heat gain test in a hot environment. Its right panel shows photographs of cargo truck models with the cargo boxes coated by the commercial white paint, plain Al MF coating, and white-BLC, respectively. (Scale bars, 5 cm.) (*E*) Measured temperature increase curves for the truck models with different surface coatings. The plain Al MF coating and white-BLC can greatly decrease the temperature increase by resisting radiative heat gain from the ambient. (*F*) Measured ice mass during the testing period of additional heat gain test. The plain Al MF coating and white-BLC apparently slowed down the melting speed of ice. The Inset illustrates the test: the same cargo truck models were used and tested in the 40 °C environment, but ice cubes as phase change materials buffering thermal exchange were loaded into the cargo boxes for comparison. (*G*) Photographs showing the melting of ice cubes in the cargo boxes with different surface coatings in a 40-min testing period.

temperature once the samples were put into the hot environment. The plain Al MF paint and white-BLC both led to a much slower inner temperature increase in contrast to the commercial white paint, as exhibited in Fig. 4*E*. It well verifies that the high thermal reflectance of these paints can effectively alleviate radiative heat gain from the ambient. Plus, we performed tests to characterize the mass change of phase change materials that are usually utilized during cold-chain transportation. Ice cubes were chosen as a representative of phase change material and were stored inside the cargo boxes in the same hot ambient environment (*Inset* of Fig. 4*F*). Fig. 4*F* shows the measured ice mass, and Fig. 4*G* exhibits the photographs of ice cubes before and after the 40-min testing period (*SI Appendix*, Fig. S11, displays photographs at an interval of 10 min). It was observed that both the plain Al MF coating and white-BLC can significantly slow down the ice melting speed by around 20.8%. At the end of the test, the mass of ice cubes inside cargo boxes with low-e coatings was approximately twice as much as the one with the commercial white paint. It indicates that a great amount of cooling energy or phase change materials for temperature maintenance can be saved during transportation.

The experiments conducted in artificial hot/cold environments effectively demonstrate the heat insulation properties of our materials. To further evaluate their cooling performance during hot days, we carried out outdoor tests under real summer weather conditions (May, California), where solar radiation and sky access were involved (see *Materials and Methods* for more details, and *SI Appendix*, Note S2 and Figs. S12–S19 *f*or additional information). We compared commercial paints with a thickness of ~10 μm (the same as BLCs) to BLCs. In our tests, BLCs resulted in lower temperatures. This is because their high NIR reflectance reduces solar heat gain, and their high MIR reflectance resists heat gain from surroundings (such as, ground). These benefits outweigh the limitation of restricted MIR radiation towards the sky.

Building HVAC Saving Simulation. In addition, we utilized commercialized building energy simulation software, EnergyPlus (version 9.5), to calculate how much HVAC energy can be saved annually for a typical midrise apartment building if the colorful low-e paints are applied to walls and roofs (see *Materials and Methods* for more details). We examined cities in different climate zones across the United States, and hourly weather data in every location for a typical meteorological year (TMY3) were utilized as external weather condition, comprehensively involving temperature, relative humidity, wind direction and speed, solar radiation, etc. The HVAC saving consists of heating energy saving, cooling energy saving, and fans energy saving. As shown in Fig. 5*A*, universal heating energy saving can be realized by installation of our colorful low-e paints because it can help reduce heat loss for indoor environments during cold days. The annual heating energy-saving value varies from 0.102 MJ/m^2/y (Kona, Hawaii) to 21.07 MJ/m^2/y (Winslow, Arizona), which is influenced not only by local weather but also by the building's insulation condition. In general, the heating energy-saving effect is more pronounced for cold climate zones and buildings with less insulation. In our simulation, the maximum heating energy savings were not observed in the coldest climate zone (Alaska), which could be attributed to the fact that the original building insulation in this area is already the best. For cooling energy savings (Fig. 5*B*), it indicates that the application of our paints exhibits a more significant effect on less-insulated buildings in hot climate zones. For instance, the annual cooling energy saving for Miami amounts to 11.37 MJ/m^2/y. It is also due to the reduced solar heating and radiative heat gain from hot surroundings (i.e., ground, in the model) that offsets the limited radiative cooling to the sky. On the other hand, installing our colorful low-e paints causes negative cooling energy savings in some cities, where the decreased sky radiative cooling by low MIR emissivity dominates. The negative effect on cooling energy saving might be relieved for buildings in urban areas, in which the

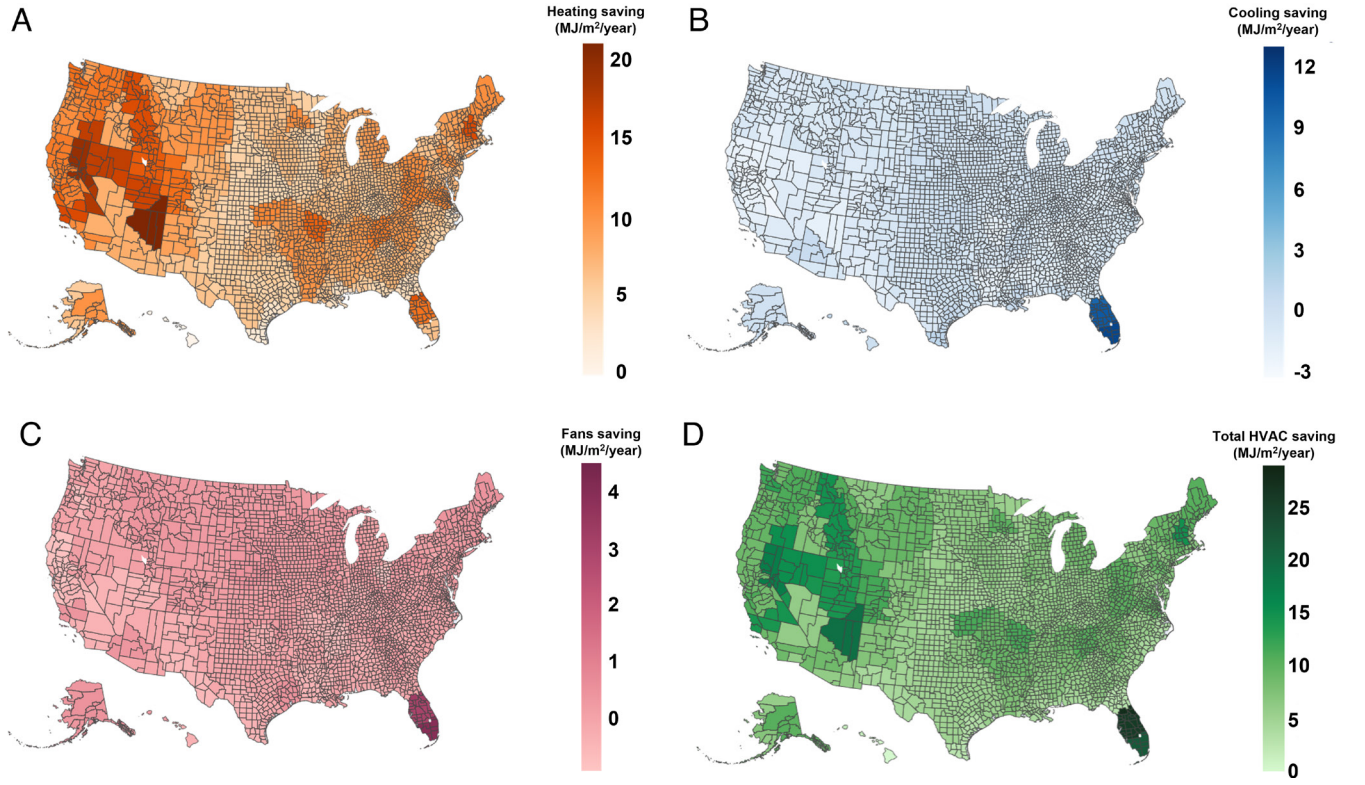

Fig. 5. Calculated energy-saving maps for a typical midrise apartment building in different climate zones across the United States, with the installation of the colorful low-e paints. (*A*) Heating savings. (*B*) Cooling savings. (*C*) Fans savings. (D) Total HVAC savings.

view factor to sky is much smaller than that of an isolated building simulated here. Fans are responsible for circulating air throughout the building, commonly used in conjunction with cooling and heating systems helping to distribute the cooled and heated air throughout the building. The installation of our low-e paints can result in fans energy savings up to 3.90 MJ/m^2/y, which is also more pronounced in hot climate zones (Fig. 5*C*). Overall, positive total HVAC energy savings can be achieved across the US by installation of our materials. As shown in Fig. 5*D*, up to 27.24 MJ/m^2/y energy can be saved annually (corresponding to the 7.4% saving ratio), and the energy-saving effect is universal across the whole country, revealing that a huge amount of electricity and natural gas can be saved and leading to greenhouse gas emission reduction. The HVAC energy-saving effect for buildings is a comprehensive result of both MIR low-emissivity and high solar reflectance, which decently balance the heating and cooling energy savings and penalties (see *SI Appendix*, Note S3 and Figs. S20 and S21 for more information). Although the optical design of our colorful low-e paints is not optimized for cooling or heating individually, it provides a more comprehensive year-round energy-saving solution that is aptly suited to a variety of regions. Despite the evident HVAC energy savings as demonstrated by EnergyPlus, it is worth mentioning that the results for Miami and its surrounding areas might be considered outliers. The U value of exterior walls in the Miami area is unusually high in the database, indicating greatly less insulation compared to other locations. This likely contributes to the "outlier" status and should be duly highlighted.

Conclusion

In summary, we reported a category of colorful low-emissivity paints that are designed to produce bilayer coatings simultaneously satisfying thermal effect as extra heat insulation through greatly reducing radiative thermal exchange and aesthetical effect for desired visual appearance. Through formulation optimization, the paints can readily generate spectrally selective coatings that not only meet optical property requirements but also demonstrate commendable hydrophobicity, environmental durability, color fastness, and cleanability, attesting to their practical application feasibility. Owing to their ~80% MIR reflectance (equivalent to 0.2 MIR emissivity), these paints have been demonstrated to effectively reduce the heating power requirements by around 36% and decrease the rate of ice melting by 20.8% within enclosed spaces subjected to artificial hot/cold environments. Compared to commercial paints, the ultrathin BLCs (10 μm) deliver higher NIR reflectance (65 to 75%), which can provide supplementary resistance to solar heating (~55% solar reflectance on average), useful for cooling in hot climates. The optical design offers a comprehensive, year-round energy-saving solution that balances the demands of both heating and cooling energy savings. Using a typical midrise apartment building as a model, energy-saving calculations based on EnergyPlus indicate a universal HVAC energy-saving effect (up to 27.24 MJ/m^2/y) across the United States. Moreover, the adaptability of our colorful low-emissivity paints ensures their suitability for a wide range of application scenarios. We expect that these paints can be readily applied to envelopes without compromising aesthetic appeal, contributing significantly to energy savings for space cooling and heating.

Materials and Methods

Materials Synthesis and Fabrication. The Al MFs used for paint formulation were used as purchased (Fisher Scientific, 99.7%). All the solvents were purchased from Fisher Scientific without further purification. Nitrile Butadiene Rubber-co-Urea (NBR-U) polymer binder was synthesized via the one-pot reaction between the primary amine-terminated nitrile butadiene rubber (NBR, Hypro 1,300 × 42, Huntsman, with 18% acrylonitrile) and hexamethylene diisocyanate (HDI, Sigma-Aldrich, 99%) in methylene chloride at 25 °C for 24 h. The as-prepared polymer Nitrile Butadiene Rubber-co-Urea (NBR-U) was dissolved in methylene chloride and purified by washing with a large amount of methanol. The final polymer NBR-U was obtained by removing the solvent under vacuum (*SI Appendix*, Fig. S3, yield 89%). The polymer NBR-U was dissolved and stored in methylene chloride with a concentration of 50 mg/mL before use. The complete Al MF paint formulation was made by mixing the Al MFs, NBR-U solution, and p-Xylene solvent, with the ratio of Al mass (g): NBR-U mass (g): solvent volume (methylene chloride and p-Xylene, mL) equal to 10:3:110. The mixture was stirred and sonicated for better dispersion. The pigment nanoparticles including PB (ACROS Organics), iron oxide (Sigma-Aldrich, 99%), goethite (Sigma-Aldrich, 30 to 63% Fe), and ZnO (Sigma-Aldrich, 99.9%) were used as purchased. The color paints were made by mixing the pigment nanoparticles, NBR-U solution, and acetone solvent with the ratio of pigment mass (g): NBR-U mass (g): solvent volume (methylene chloride and acetone, mL) = 1:0.5:110). Similarly, the mixture was stirred and sonicated for better dispersion. White, blue, red, and yellow colors were realized by a single kind of pigment, while other colors were made by mixing two or three kinds of pigment nanoparticles at a certain ratio. When preparing coatings, the solutions were loaded into a spray gun (3M) and sprayed onto substrates at room temperature. The loading mass density per unit area was calculated by weighing sample mass before and after spraying coatings and the substrate area. Commercial paints were purchased from Home Depot (blue: Glidden Premium, red: BEHR Marquee, yellow: BEHR Premium plus, and white: Glidden Premium). They were diluted by acetone and applied on substrates by the same spray coating method. The loading mass density per unit area can be calculated by the same method as above.

Material Characterization. The MIR reflectance was measured by an FTIR spectrometer (Model 6700, Thermo Scientific) accompanied by a diffuse gold integrating sphere (PIKE Technologies). ATR-FTIR spectra were measured by the Nicolet iS50 FTIR Spectrometer. The visible and NIR reflectance was measured by UV-Vis-NIR spectrometers (Agilent, Cary 6000i and Jasco V-670) equipped with diffuse reflectance accessories. SEM images were taken by FEI Nova NanoSEM (5 kV). The contact angle was measured by a contact angle goniometer (Rame-Hart 290). The sample mass was measured by an analytical balance (Ohaus Pioneer, 0.0001g readability).

Environmental Durability Tests. 1) High-temperature test: the sample was put into an oven (MTI, SS-00AB table dry oven) at a constant temperature of 80 °C and maintained for 1 wk; 2) Low-temperature test: the sample was put in a Dewar filled with liquid nitrogen for 1 wk. The tested sample was soaked in liquid nitrogen during the whole testing process; 3) Acid test: concentrated sulfuric acid (95 to 98%, Sigma-Aldrich) was diluted with deionized water. Its pH was adjusted to be around pH = 4 (tested by pH test strips, EMD Millipore). The sample was immersed in the solution continuously for 1 wk; 4) Alkali test: potassium hydroxide solution (pH = 10, tested by pH test strips, EMD Millipore) was prepared by potassium hydroxide (Sigma-Aldrich) and deionized water. The sample was immersed in the solution continuously for 1 wk. The MIR spectra of samples were measured, and photographs were taken before and after tests.

Color Fastness Test. The test method was modified from ASTM D7377. The sample was fixed with a tilt angle of ~45° at a distance of 5 cm from the water faucet. The flow rate of water from the faucet was ~300 mL/min. Water hit on the sample and then flew into the sink. Sample mass was measured at time intervals.

Heat Insulation Performance Demonstration in Artificial Cold/Hot Environments. 1) Artificial cold environment test–The building simulants with 5 cm side lengths were assembled by clear acrylic boards (1.5 mm thick, McMaster-Carr). Their bottom faces were insulation foams. Polyimide insulated flexible heaters (McMaster-Carr, ~25 cm^2) connected to a power supply (Keithley 2400) were fixed in the building simulants to provide heating power. Small holes (1 mm in diameter) were cut by a CO_2 laser cutter (Epilog Fusion M2) for inserting thermocouples (K type, Omega Engineering) into the building simulants. A data logger (HH374, Omega Engineering) was used to record the temperature data of the building simulants. The air temperature in the enclosed chamber

(artificial cold environment) was measured by a thermocouple (K type, Omega Engineering) as well, and it was controlled at 5 °C by a circulated water system. The supplied power density was adjusted for different surface coatings to make the inside temperature of the building simulants stable at 25 °C. 2) Artificial hot environment test–The cargo truck models were purchased from Amazon. The dimension of the cargo box is 23.5 cm × 4.5 cm × 3.6 cm. We added different coatings to the cargo box outer surfaces (three faces). Similarly, thermocouples (K type, Omega Engineering) were put into the cargo boxes, and they were connected to a data logger (HH374, Omega Engineering). The air temperature in the enclosed chamber (artificial hot environment) was measured by a thermocouple (K type, Omega Engineering) as well, and it was controlled at 40 °C by a circulated water system. The temperature increase curves were recorded once the truck models were put into the enclosed chamber. For the ice test, ice cubes of nearly the same mass and shape were put in a top-open acrylic container with bottom heat insulated, and the acrylic container was transferred into the cargo boxes. At certain time intervals, the ice container was taken out for photographs, and ice mass was measured by taking out and absorbing surface liquid water rapidly. For the building simulants and cargo truck models with different surface coatings, we fixed their position in the artificial hot/cold environments, as well as the position of thermocouples, heaters, and ice cube containers, to make the measurements as parallel as possible to provide reasonable comparison.

Energy-Saving Calculation by EnergyPlus. EnergyPlus (version 9.5) was used to perform whole building energy simulation. We used the commercial reference building model (post-1980 midrise apartment) defined by US DOE. The model building has four stories, including 31 apartments plus an office. The building shape is rectangular with an aspect ratio of 2.74 (length: 46.33 m, width: 16.91 m, and height: 12.19 m). Building North axis is 0 degree to true North. The total floor area is 3,135 m^2. The windows cover 15% of the total wall surface area. The building is isolated (i.e., no neighboring buildings/objects). Internal gains and HVAC systems have been comprehensively designed in the models. For the HVAC systems in the building, DX cooling is employed for cooling (COP = 3.13), while gas furnaces (burner efficiency = 0.8) and electric heaters (efficiency = 1) are used for heating. The fan's efficiency is 0.536. The indoor air temperature set-point was set constantly as 22 °C, and the external weather utilized hourly weather data for a TMY3 of different cities. The weather data comprehensively include temperature, relative humidity, wind direction and speed, solar radiation, etc. The wall and roof insulation condition of the modeled building is defined in the downloaded EnergyPlus models for 16 cities (Miami, Houston, Phoenix, Atlanta, Los Angeles, Las Vegas, San Francisco, Baltimore, Albuquerque, Seattle, Chicago, Boulder, Minneapolis, Helena, Duluth, and Fairbanks). The insulation condition varies in different locations (see U-values in *SI Appendix*, Table S1). The building insulation conditions in other cities are extrapolated from the above 16 cities. The baseline HVAC energy use, including cooling, heating, and fans, was calculated for the building model with conventional wall and roof properties (as set in the downloaded EnergyPlus models). The initial solar reflectivity values of the building exterior wall, interior wall, and roof are 0.22, 0.08, and 0.3, respectively, and MIR emissivity (thermal absorbance) values are all 0.9. To calculate the HVAC energy use with installation of our colorful low-e paints, we modified optical properties of the wall and roof surfaces (both inside and outside sides) in the building model, using experimental measured data (solar reflectivity: 0.55, MIR emissivity: 0.23. They are both average values of low-e paints in blue, red, yellow, and white). Comparing the energy use difference between building models with and without colorful low-e paint installation, we obtained the all-year energy saving for cooling, heating, fans, and total HVAC. In total, we tested 129 cities across the United States using EnergyPlus. The energy-saving map was plotted on the basis of EnergyPlus calculations for 129 cities across the United States and extrapolating to neighboring counties. All annual energy-saving values are normalized by being divided by total floor area of the simulated building (3,135 m^2).

Outdoor Tests. All the tests were performed on a flat building roof in Stanford, CA, in May 2022. For the coating samples on flat film substrates, acrylic boxes (dimension: 21 cm × 21 cm × 6.5 cm) were made, with open windows (5 cm × 5 cm) on the top side. All the surfaces of the boxes were covered with Mylar foil. Styrofoam (thickness: 5.1 cm) was fixed on the bottom of acrylic boxes. On top of the styrofoam, an aerogel blanket (dimension: 10 cm × 10 cm × 0.8 mm) was placed. All the exposed surfaces of the foam and aerogel blanket were covered with Mylar foil. The substrates for coating samples were modified polyester films (5 cm × 5 cm × 300 μm), with black color and solar absorbance of ~0.8. We set the solar absorbance at this value according to the exterior wall material parameter in the commercial reference building model (post-1980 midrise apartment) defined by US DOE in EnergyPlus version 9.5. Sample coatings were applied to the substrates by controlling the same thickness (~10 μm). Samples were mounted above the aerogel blanket with a gap of ~2 mm, facing the open windows of the boxes. Thermocouples (K type, Omega Engineering) were attached to the bottom side of sample substrates and connected to a data logger (HH374, Omega Engineering). Infrared transparent low-density polyethylene films covered the open windows right above samples during tests. In testing scenario 1, the testing boxes were put on a horizontal platform (distance to the ground, ~0.75 m). In testing scenarios 2 and 3, the testing boxes were fixed in the vertical direction to the ground (distance to the ground, ~0.5 m). Air and ground temperature was recorded by thermocouples (K type, Omega Engineering) exposed in air and fixed into the roof ground surface (crushed stones). For tests of cargo truck models, the cargo boxes were modified to be solar opaque (solar absorbance ~0.8) as well, and then, coatings were applied onto three faces of the cargo boxes (Fig. 5*D*). Thermocouples (K type, Omega Engineering) were inserted into the cargo boxes and fixed at the center of boxes. The truck models were placed on Styrofoam wrapped with Mylar foil, sitting on a heat insulation platform (Styrofoam, thickness: ~10 cm) with the solar opaque surface. The truck models were totally exposed to air without any convection shield during the tests. A thermocouple was attached onto the surface to record ground temperature, and another thermocouple in air was used to measure air temperature. Thermocouples were connected to a data logger (TC-8, Omega Engineering). Solar irradiance was measured using a pyranometer (Kipp & Zonen CMP6), and a data logger rated to a directional error of ±20 W/m^2 was used to record data. The pyranometer was placed on the roof ground.

Data, Materials, and Software Availability. All study data are included in the article and/or supporting information.

ACKNOWLEDGMENTS. Part of this work was performed at the Stanford Nano Shared Facilities and the Stanford Nanofabrication Facility. Y.C. acknowledges the support from Oriental Yuhong North American LLC.

Author affiliations: [a]Department of Materials Science and Engineering, Stanford University, Stanford, CA 94305; [b]Department of Chemical Engineering, Stanford University, Stanford, CA 94305; [c]E. L. Ginzton Laboratory, Department of Electrical Engineering, Stanford University, Stanford, CA 94305; and [d]Stanford Institute for Materials and Energy Sciences, SLAC National Accelerator Laboratory, Menlo Park, CA 94025

1. E. Pennisi, Living with heat. *Science* **370**, 778–781 (2020).
2. L. Yang, H. Yan, J. C. Lam, Thermal comfort and building energy consumption implications–A review. *Appl. Energy* **115**, 164–173 (2014).
3. N. R. Jankowski, F. P. McCluskey, A review of phase change materials for vehicle component thermal buffering. *Appl. Energy* **113**, 1525–1561 (2014).
4. S. Chu, A. Majumdar, Opportunities and challenges for a sustainable energy future. *Nature* **488**, 294–303 (2012).
5. X. Yin, R. Yang, G. Tan, S. Fan, Terrestrial radiative cooling: Using the cold universe as a renewable and sustainable energy source. *Science* **370**, 786–791 (2020).
6. N. Oreskes, The scientific consensus on climate change. *Science* **306**, 1686–1686 (2004).
7. E. A. Goldstein, A. P. Raman, S. Fan, Sub-ambient non-evaporative fluid cooling with the sky. *Nat. Energy* **2**, 1–7 (2017).
8. S. Baldwin *et al.*, "Chapter 5: Increasing efficiency of building systems and technologies" in *Quadrennial Technology Review: An Assessment of Energy Technologies and Research Opportunities* (U.S. Department of Energy, 2015), pp. 145–182.
9. Y. Peng *et al.*, Nanoporous polyethylene microfibres for large-scale radiative cooling fabric. *Nat. Sustain.* **1**, 105–112 (2018).
10. X. Li *et al.*, Integration of daytime radiative cooling and solar heating for year-round energy saving in buildings. *Nat. Commun.* **11**, 6101 (2020).
11. W. Goetzler *et al.*, *Energy Savings Potential and RD&D Opportunities for Commercial Building HVAC Systems* (U.S. Department of Energy, 2017).
12. L. Filina-Dawidowicz, S. Filin, Innovative energy-saving technology in refrigerated containers transportation. *Energy Effic.* **12**, 1151–1165 (2019).
13. Y. Li *et al.*, Multifunctional organic-inorganic hybrid aerogel for self-cleaning, heat-insulating, and highly efficient microwave absorbing material. *Adv. Funct. Mater.* **29**, 1807624 (2019).

14. B. Wicklein *et al.*, Thermally insulating and fire-retardant lightweight anisotropic foams based on nanocellulose and graphene oxide. *Nat. Nanotechnol.* **10**, 277–283 (2015).
15. R. Baetens *et al.*, Vacuum insulation panels for building applications: A review and beyond. *Energy Build.* **42**, 147–172 (2010).
16. B. P. Jelle, Traditional, state-of-the-art and future thermal building insulation materials and solutions–Properties, requirements and possibilities. *Energy Build.* **43**, 2549–2563 (2011).
17. A. Synnefa, M. Santamouris, I. Livada, A study of the thermal performance of reflective coatings for the urban environment. *Sol. Energy* **80**, 968–981 (2006).
18. I. Hernández-Pérez *et al.*, Thermal performance of reflective materials applied to exterior building components–A review. *Energy Build.* **80**, 81–105 (2014).
19. B. P. Jelle *et al.*, Fenestration of today and tomorrow: A state-of-the-art review and future research opportunities. *Sol. Energy Mater. Sol. Cells* **96**, 1–28 (2012).
20. B. P. Jelle, S. E. Kalnæs, T. Gao, Low-emissivity materials for building applications: A state-of-the-art review and future research perspectives. *Energy Build.* **96**, 329–356 (2015).
21. P. Principi, R. Fioretti, Thermal analysis of the application of PCM and low emissivity coating in hollow bricks. *Energy Build.* **51**, 131–142 (2012).
22. S. Fantucci, V. Serra, Low-E paints enhanced building components: Performance, limits and research perspectives. *Energy Procedia* **126**, 274–281 (2017).
23. S. Fantucci, V. Serra, Experimental assessment of the effects of low-emissivity paints as interior radiation control coatings. *Appl. Sci.* **10**, 842–857 (2020).
24. A. Joudi, H. Svedung, M. Cehlin, M. Rönnelid, Reflective coatings for interior and exterior of buildings and improving thermal performance. *Appl. Energy* **103**, 562–570 (2013).
25. A. J. Elliot, M. A. Maier, Color psychology: Effects of perceiving color on psychological functioning in humans. *Annu. Rev. Psychol.* **65**, 95–120 (2014).
26. S. E. Palmer, K. B. Schloss, J. Sammartino, Visual aesthetics and human preference. *Annu. Rev. Psychol.* **64**, 77–107 (2013).
27. Y. Chen *et al.*, Colored and paintable bilayer coatings with high solar-infrared reflectance for efficient cooling. *Sci. Adv.* **6**, eaaz5413 (2020).
28. L. Cai *et al.*, Temperature regulation in colored infrared-transparent polyethylene textiles. *Joule* **3**, 1478–1486 (2019).
29. W. Li, Y. Shi, Z. Chen, S. Fan, Photonic thermal management of coloured objects. *Nat. Commun.* **9**, 4240 (2018).
30. Y. Peng *et al.*, Coloured low-emissivity films for building envelopes for year-round energy savings. *Nat. Sustain.* **5**, 339–347 (2022).
31. F. N. Jones, M. E. Nichols, S. P. Pappas, "Chapter 20: Pigments" in *Organic Coatings: Science and Technology* (John Wiley & Sons Inc, 2006), pp. 293–306.
32. L. Cai *et al.*, Spectrally selective nanocomposite textile for outdoor personal cooling. *Adv. Mater.* **30**, 1802152 (2018).